Immune Netw. 2022 Jun;22(3):e27
https://doi.org/10.4110/in.2022.22.e27
pISSN 1598-2629·eISSN 2092-6685

IMMUNE NETWORK

Brief Communication

Check for updates

Characterization of Immune Cells From the Lungs of Patients With Chronic Non-Tuberculous Mycobacteria or *Pseudomonas aeruginosa* Infection

Alan R. Schenkel [1,*], John D. Mitchell[2], Carlyne D. Cool[3,4], Xiyuan Bai[5,6], Steve Groshong[3,4], Tilman Koelsch[7], Deepshikha Verma [1], Diane Ordway [1], Edward D. Chan[5,6,8,9]

[1]Department of Microbiology, Immunology, & Pathology, Colorado State University, Fort Collins, CO 80523, USA
[2]Division of Cardiothoracic Surgery, University of Colorado Anschutz Medical Campus, Aurora, CO 80045, USA
[3]Department of Pathology, National Jewish Health, Denver, CO 80206, USA
[4]Department of Pathology, University of Colorado Anschutz Medical Campus, Aurora, CO 80045, USA
[5]Department of Academic Affairs, National Jewish Health, Denver, CO 80206, USA
[6]Division of Pulmonary Sciences and Critical Care Medicine, University of Colorado Anschutz Medical Campus, Aurora, CO 80045, USA
[7]Department of Radiology, National Jewish Health, Denver, CO 80206, USA
[8]Department of Medicine, National Jewish Health, Denver, CO 80206, USA
[9]Pulmonary Section, Rocky Mountain Regional Veterans Affairs Medical Center, Aurora, CO 80045, USA

Received: Dec 12, 2021
Revised: Mar 14, 2022
Accepted: Mar 15, 2022
Published online: Apr 11, 2022

***Correspondence to**
Alan R. Schenkel
Department of Microbiology, Immunology, & Pathology, Colorado State University, Microbiology B222B, 1682 Campus Delivery, Fort Collins, CO 80523, USA.
Email: Alan.Schenkel@colostate.edu

ORCID iDs
Alan R. Schenkel
https://orcid.org/0000-0002-1603-5713
Deepshikha Verma
https://orcid.org/0000-0002-8549-6409
Diane Ordway
https://orcid.org/0000-0003-0003-326X

Conflict of Interest
The authors declare no potential conflicts of interest.

ABSTRACT

Little is known of the lung cellular immunophenotypes in patients with non-tuberculous mycobacterial lung disease (NTM-LD). Flow-cytometric analyses for the major myeloid and lymphoid cell subsets were performed in less- and more-diseased areas of surgically resected lungs from six patients with NTM-LD and two with *Pseudomonas aeruginosa* lung disease (*PsA*-LD). Lymphocytes, comprised mainly of NK cells, $CD4^+$ and $CD8^+$ T cells, and B cells, accounted for ~60% of all leukocytes, with greater prevalence of T and B cells in more-diseased areas. In contrast, fewer neutrophils were found with decreased number in more-diseased areas. Compared to NTM-LD, lung tissues from patients with *PsA*-LD demonstrated relatively lower numbers of T and B lymphocytes but similar numbers of NK cells. While this study demonstrated a large influx of lymphocytes into the lungs of patients with chronic NTM-LD, further analyses of their phenotypes are necessary to determine the significance of these findings.

Keywords: Leukocytes; Lung; Non-tuberculous mycobacteria; Pseudomonas aeruginosa; Lymphocytes

INTRODUCTION

The radiographic manifestations of non-tuberculous mycobacterial lung disease (NTM-LD) is often classified into three main types although overlaps may be seen: (i) nodules and bronchiectasis ("nodular-bronchiectasis disease") that often involve the right middle lobe, lingula, and/or right upper lobe, (ii) nodular-bronchiectasis pattern with cavitation in one

IMMUNE NETWORK

Abbreviations

BAL, bronchoalveolar lavage; CT, computed tomography; MAC, *Mycobacterium avium* complex; NTM, non-tuberculous mycobacterial; NTM-LD, non-tuberculous mycobacterial lung disease; *PsA*-LD, *Pseudomonas aeruginosa* lung disease.

Author Contributions

Conceptualization: Schenkel AR, Ordway D, Chan ED; Data curation: Schenkel AR, Mitchell JD, Cool CD, Chan ED; Formal analysis: Schenkel AR, Cool CD; Funding acquisition: Ordway D; Investigation: Schenkel AR, Mitchell JD, Cool CD, Bai X, Groshong S, Koelsch T, Verma D, Ordway D, Chan ED; Methodology: Schenkel AR, Mitchell JD, Cool CD, Bai X, Groshong S, Koelsch T, Verma D, Ordway D, Chan ED; Resources: Mitchell JD, Cool CD, Bai X, Groshong S, Koelsch T, Verma D, Ordway D, Chan ED; Writing - original draft: Schenkel AR, Ordway D, Chan ED; Writing - review & editing: Schenkel AR, Mitchell JD, Cool CD, Bai X, Groshong S, Koelsch T, Verma D, Ordway D, Chan ED

or more of the nodules, and (iii) fibrocavitary disease affecting the upper lobes in the setting of underlying emphysema. Other radiographic features of NTM-LD include inflammatory bronchiolitis manifesting as branching centrilobular nodules (tree-in-bud opacities), atelectasis, ground glass opacities, and/or consolidation.

Correlation of these radiographic features with histopathology can provide greater insights into the cellular pathogenesis of NTM-LD (1-3). For example, in resected lung tissues, computed tomography (CT) findings of bronchiectasis and bronchiolitis correlated with peribronchial and peribronchiolar granulomatous inflammation, respectively, as well as with airway wall necrosis (1). Lung nodules and cavity walls were also found to be comprised of caseating granulomas; interestingly, the outer rim of cavity walls may be surrounded by myofibroblasts, the differentiation of which requires the immunosuppressive cytokine TGF-β (1).

More detailed analysis of the lung cellular composition may shed further light on the pathogenesis of NTM-LD. When examining lung histopathologic tissues of those NTM-LD, we observed prominent infiltration by numerous lymphocytes but could not find in the literature characterization of their phenotypes. Surgical resection of non-tuberculous mycobacterial (NTM) diseased segment or lobe (or sometimes an entire lung) is routinely executed in some centers (4,5). While prospective, randomized control studies have not been performed on such treatment, surgical resection in selected patients – typically those with severe but localized disease – have been associated with improved microbiologic outcome (6-9). Surgical lung resection has also been shown to be salubrious for individuals with multi-drug resistant tuberculosis (10,11). While standard histopathologic analyses can provide information on the major cell types and the architecture of the pathology, it does not discriminate stringently or quantify the immune cell phenotypes involved in the pathologic process. Indeed, we are unaware of detailed cellular analyses in the actual lung tissues of pulmonary NTM patients. Thus, we undertook a pilot study to analyze and correlate the radiographic, histopathologic, and immune cell phenotypes, the lattermost as determined by flow cytometry, of the surgically-removed lung tissues of six patients with NTM-LD and compared the findings to that of two patients with chronic *Pseudomonas aeruginosa* lung disease (*PsA*-LD). In this study, large numbers of smaller lymphocytes, comprised of $CD4^+$ T cells, $CD8^+$ T cells, and both $CD16^+$ and $CD56^+$ NK cells were found in NTM-LD. Infiltration by $CD19^+$ B cells varied widely. Contrary to our expectations, there were relatively few neutrophils in the lung tissues.

MATERIALS AND METHODS

Patient identification

Following Institutional Review Board approval (National Jewish Health HS# 3137), six patients with NTM-LD were prospectively identified to be undergoing lung resection. For comparison, two patients with chronic *PsA*-LD but no history of NTM-LD who were having lung resection were also included. Each patient underwent lung surgery as part of their recommended treatment.

CT scan and lung histopathologic images

The pre-surgical chest CT scan closest to the time of the surgery and the surgical histopathology were analyzed. The histopathologic slides of the post-surgical lung specimens

sent to the Pathology Department and prepared by the clinical histopathology laboratory were examined and representative images were obtained.

Procurement of fresh lung tissues

For each surgically removed lung specimen, two-1 cm^3 lung pieces were excised in the operating room from areas that visually appeared to be less affected ("less-diseased") and two pieces from areas that appeared severely affected ("more-diseased"). The lung tissues were immediately placed in cold Hanks Buffered Saline Solution, kept at 4°C, and processed for flow cytometry within 24 h.

Flow cytometry and gating scheme

From each pair of less-diseased and more-diseased samples, one piece was fixed and stained for histology with H&E. The other paired lung tissue samples were digested in ~2 units DNAse I, ~5 mg collagenase, and 10 ml RPMI buffer with no serum. Five ml was used for each tissue sample and digested for 30 min at 37°C with occasional mixing. The digestion was stopped with addition of 5 ml cold RPMI (4°C) with 10% FBS, the cells separated from the larger tissue matrix debris through a 70 μm filter, and the recovered cells centrifuged and counted on a hemocytometer. A total of 200,000 cells were stained in each tube for extracellular markers and live/dead cells. Cell surface markers were used to identify granulocytes ($SSC^{high}CD14^{-}CD66b^{+}$), macrophages ($SSC^{high}CD14^{+}CD66b^{-}$), monocytes ($SSC^{medium}CD14^{+}CD66b^{-}$), large lymphocytes ($SSC^{high/medium}$), and small lymphocytes (SSC^{low}) as well as lymphocytic phenotypes NK cells (SSC^{high}, $CD16^{high}$ vs. $CD56^{+}$), T cells ($CD3^{+}$, $CD4^{+}$, $CD8^{+}$, pan-gamma/delta T cell $receptor^{+}$), and B cells ($CD19^{+}$). Cells were fixed and collected on a Becton Dickinson FACS Canto II, and the data analyzed by FloJo.

We gated first on forward scatter and side scatter, followed by CD45 and live-dead violet to find the live $CD45^{+}$ populations. Forward and side scatter plots were also used to examine relative granularity and size of each cell population.

Statistics

Data were analyzed in Prism 8.2 with paired *t*-test statistics to each subset, comparing paired (less-diseased vs more-diseased) samples from each patient.

RESULTS AND DISCUSSION

Demographics, NTM species, and type of lung resection

The gender, age at the time of surgery, key past medical history, the peripheral white blood cell count and differential closest to the time of surgery, the responsible NTM species, and the resected part of the lung are recorded in **Table 1**. All the patients were women and *Mycobacterium avium* complex (MAC) species accounted for all of the NTM-LD analyzed. Similar demographic information was also recorded for the two patients with *PsA*-LD (**Table 1**). The peripheral white blood cell count was within normal limits in all patients except for patient B, where it was only very slightly elevated. The percent neutrophils and lymphocytes in the peripheral blood were essentially within normal limits.

Correlation of high-resolution CT scan with histopathology

The most representative axial chest CT image and the key histopathologic photomicrograph (H&E) for each of the NTM-LD patients are shown in **Fig. 1**. Of the six patients with NTM-

Table 1. Clinical, microbiologic, and surgical data of six subjects with NTM-LD and two with *PsA*-LD

Patient	Age (yr), sex	Past medical history	WBC and differential* (cells/L & %)	NTM species	Lung segment or lobe removed
A	49F	PiMZ, GERD, esophageal dyskinesia, vitamin D deficiency, vitiligo	5.9×10^9 $P^{59}L^{27}M^{7}E^{6}$	*M. intracellulare* & *M. yongonense*	Posterior segment of RUL
B	67F	Prior left apical lung segmentectomy, cardiomyopathy, emphysema, esophageal dyskinesia, GERD, hypertension, fibromuscular dysplasia, hypothyroidism, LBBB, SS-B Ab (+)	11.4×10^9 $P^{77}L^{12}M^{9}E^{1}$	*M. intracellulare*	Completion left pneumo-nectomy
C	37F	Chronic sinusitis	10×10^9 $P^{70}L^{18}M^{9}E^{3}$	Macrolide-resistant MAC	RUL
D	64F	Asthma, GERD, depression, rheumatic fever, osteoporosis, mitral valve prolapse, scoliosis, hearing loss	5.8×10^9 $P^{70}L^{18}M^{9}E^{3}$	*M. intracellulare*	LLL
E	61F	Asthma, GERD, irritable bowel syndrome, depression, osteoporosis	7.7×10^9 $P^{75}L^{11}M^{11}$	MAC	Lingula
F	65F	GERD, hypothyroidism	9.5×10^9 $P^{66}L^{20}M^{12}E^{1}$	MAC	RML
G	74F	Chronic *P. aeruginosa* lung infection, esophageal dyskinesia, GERD, hypothyroidism	8.4×10^9 $P^{75}L^{11}M^{11}$	No history of NTM	RML
H	63F	Chronic *P. aeruginosa* lung infection, allergic rhinitis, GERD, sicca syndrome (SS-A Ab +), hypothyroidism, sinusitis	8.6×10^9 $P^{70}L^{18}M^{10}E^{3}$	No history of NTM	Lingula SS-LLL

GERD, gastroesophageal reflux disease; LBBB, left bundle branch block; LLL, left lower lobe; PiMZ, protease inhibitor MZ phenotype; RML, right middle lobe; RUL, right upper lobe; SS, superior segment; WBC, white blood cell (normal WBC range [4–10×10^3/L].
*Normal neutrophil percent range (42%–78%) and normal lymphocyte percent range (13%–41%).

LD, five were classified as having nodular-bronchiectasis pattern on chest CT and one had fibrocavitary disease. Histopathologically, necrotizing granuloma were seen in four (**Fig. 1A-D**), non-necrotizing granuloma were seen in one (**Fig. 1E**), and dilated small airways with peribronchiole and/or intraluminal inflammation were seen in all although may not be apparent in the photomicrographs shown. Two lung specimens were notable for relatively large, discrete nodules composed of necrotizing granulomas (**Fig. 1C and D**). Of the two patients with chronic *PsA*-LD, nodular-bronchiectasis were seen in both (**Fig. 1G and H**); histopathologic analysis was notable for dilated bronchioles with surrounding fibrosis with peribronchiole and intraluminal inflammation but no granulomas. Additional CT images and histopathologic photomicrographs for each of these eight patients are shown in **Supplementary Figs. 1-8**. It is important to emphasize that the histopathologic images shown in **Figs. 1** and **2** and in the Supplementary Figures were from histopathology slides prepared by the clinical pathology laboratory at the University of Colorado Anschutz Medical Campus as part of the clinical pathologic evaluation.

Separate pieces of lung tissues obtained for flow cytometric analysis were also prepared with H&E staining for histopathologic analysis. We found that there was a very substantial mononuclear population, many of them relatively small lymphocytes (**Fig. 2**). These cells were found in clusters or scattered among largely fibrotic tissue and were more abundant in more-diseased areas. It was also quite apparent that neutrophils were not a significant component of the infiltrate, which is actually not inconsistent with the bronchoalveolar lavage (BAL) analysis of stable MAC lung disease wherein macrophages were found in greater numbers than lymphocytes and both greater than neutrophils (12).

Flow cytometric analyses

For the flow cytometric analyses, two different Ab panels were used, one for the major leukocyte subsets and the other for the major lymphocyte subsets with conventional markers (13). For the NTM-LD tissues, analysis revealed that both the percentage and absolute number of neutrophils were the lowest among all cell types examined in both the less-diseased and more-diseased

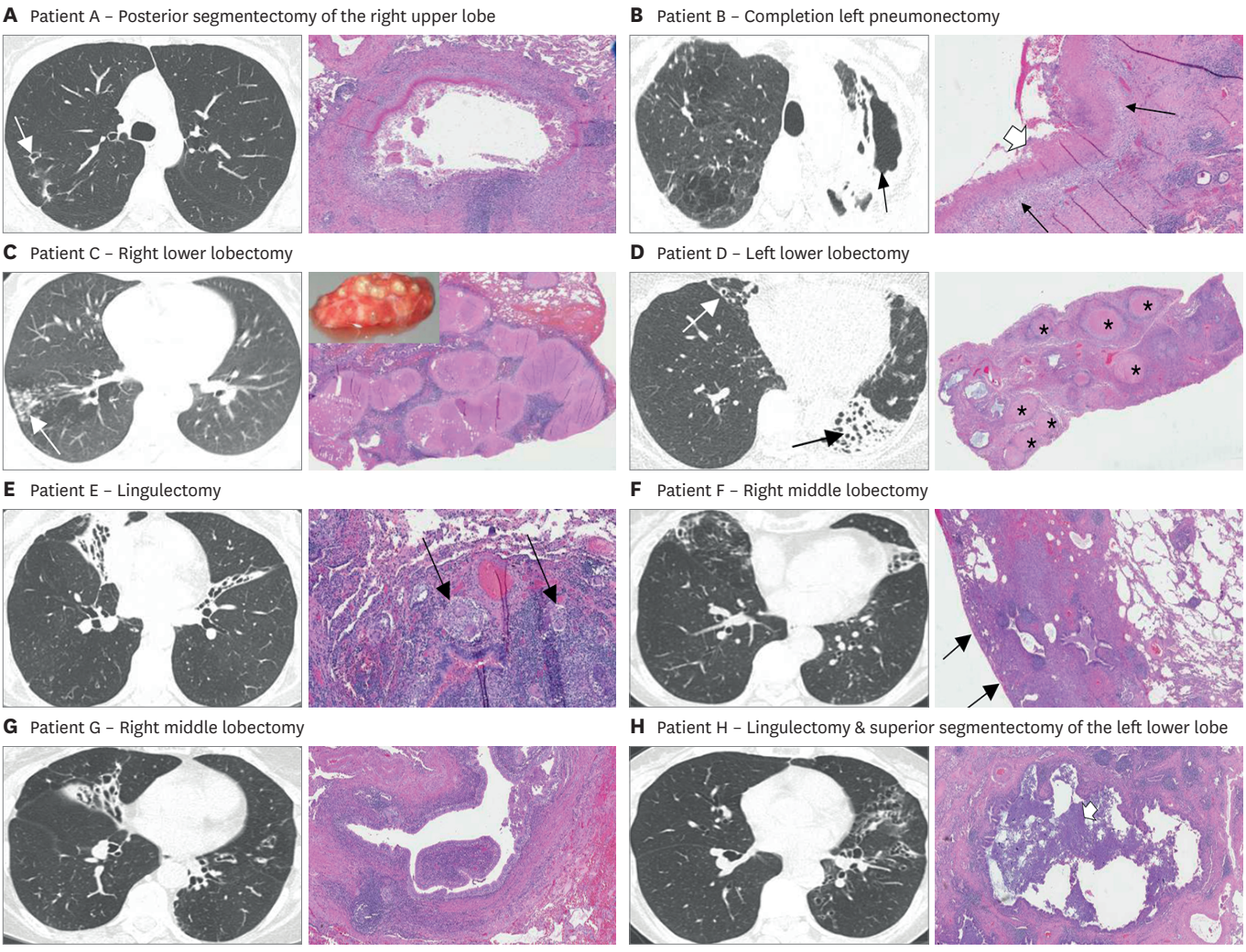

Figure 1. Representative axial CT image and the key histopathologic photomicrograph (H&E) for six patients with NTM lung disease. (A) Axial CT image shows a small cavity in the posterior segment of the right upper lobe and some surrounding tree-in-bud opacities. The lung photomicrograph demonstrates necrotizing granuloma with central necrotic material surrounded by epithelioid histiocytes, multinucleated giant cells and chronic inflammation, including lymphoid aggregates. (B) Axial CT image shows severe left upper lobe fibrocavitary disease with significant volume loss. The lung photomicrograph demonstrates necrotizing granuloma with layers of necrosis (thick white arrow), epithelioid histiocytes (thin black arrows) and surrounding fibrosis and chronic inflammation. (C) Axial CT image shows a bronchiectatic airway in the right lower lobe with numerous coalescing small to medium size nodules distally (arrow). The lung photomicrograph demonstrates numerous coalescing, necrotizing granulomas. Inset is the gross surgical tissue sample analyzed demonstrating the visible nodular lesions that corresponded to both the nodules found on the CT scan and the relatively large, nodular granulomas seen on histopathology. (D) Axial CT image shows severe bronchiectasis and atelectasis of the left lower lobe (black arrow) and moderate bronchiectasis in the right middle lobe (white arrow). The lung photomicrograph (low power) demonstrates numerous necrotizing granuloma (asterisks) with central necrosis surrounded by fibrosis and chronic inflammation. (E) Axial CT image shows severe bronchiectasis and atelectasis in the right middle lobe and in the superior segment of the lingula. The lung photomicrograph demonstrates an airway wall with chronic inflammation that includes lymphoid aggregates and nonnecrotizing granulomas with multinucleated giant cells (black arrows). (F) Axial CT image shows bronchiectasis and tree-in-bud opacities of the right middle lobe and atelectasis/bronchiectasis of the lingula. The lung photomicrograph demonstrates peripheral area of fibrosis (note the pleural surface—thin black arrows) surrounding mildly dilated small airway with lymphoid aggregates in the airway wall. Representative axial CT image and the key histopathologic photomicrograph (H&E) for two patients with chronic *PsA*-LD. (G) Axial CT image shows bronchiectasis of the central airways and the right middle lobe. The lung photomicrograph demonstrates dilated bronchiole, surrounded by collagenous fibrosis. (H) Axial CT image shows diffuse bronchiectasis of the left upper lobe and central region of the left lower lobe. The lung photomicrograph demonstrates a dilated small airway with inflammatory debris within the lumen (white arrow) with peripheral area of dense fibrosis.
Additional CT images and lung photomicrographs are shown in **Supplementary Figs. 1-8**.

samples with no significant difference between the two areas (**Fig. 3A and B**). While macrophage and monocyte numbers were higher than for the neutrophils, there was no quantitative difference in each of these two mononuclear cell types between the less- and more-diseased samples. There was a trend toward greater absolute number of large lymphocytes in the more-

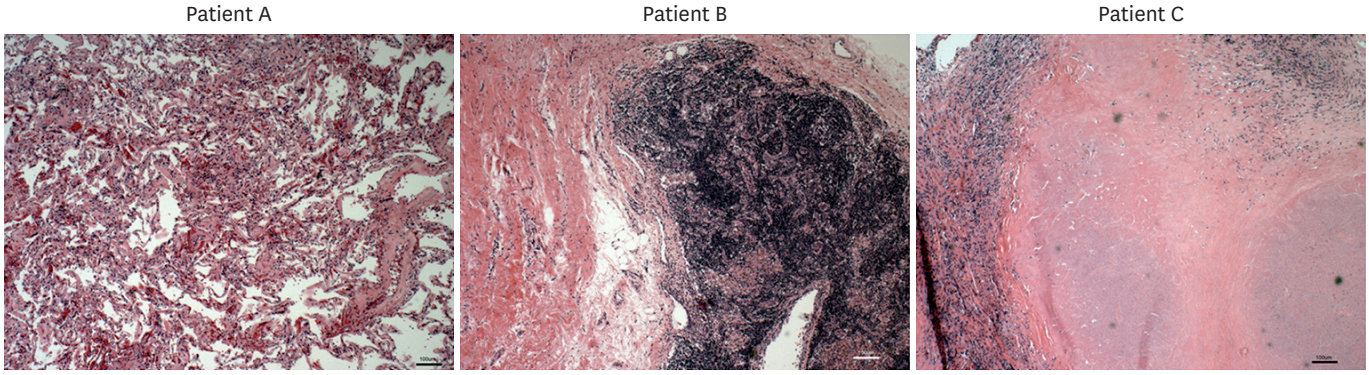

Figure 2. Typical histology of 1 cm³ lung tissues of three NTM-LD patients showing abundant number of lymphocytes. Lymphocytes were typically found more diffusely across the tissues but occasionally in varied sized clusters, sometimes quite large (middle panel). Note the apparent lack of neutrophils.
PMN, polymorpho-neutrophils; Mono, monocytes; LL, large lymphocytes; SL, small lymphocytes.
*p<0.05.

diseased areas (**Fig. 3B**). Significantly greater percentage of small lymphocytes were seen in the more-diseased samples compared to the less-diseased areas, and a trend toward greater absolute numbers (**Fig. 3A and B**). Both CD16⁺ and CD56⁺ NK cells could be found in relatively large numbers, but there no significant difference between the less- and more-diseased tissues.

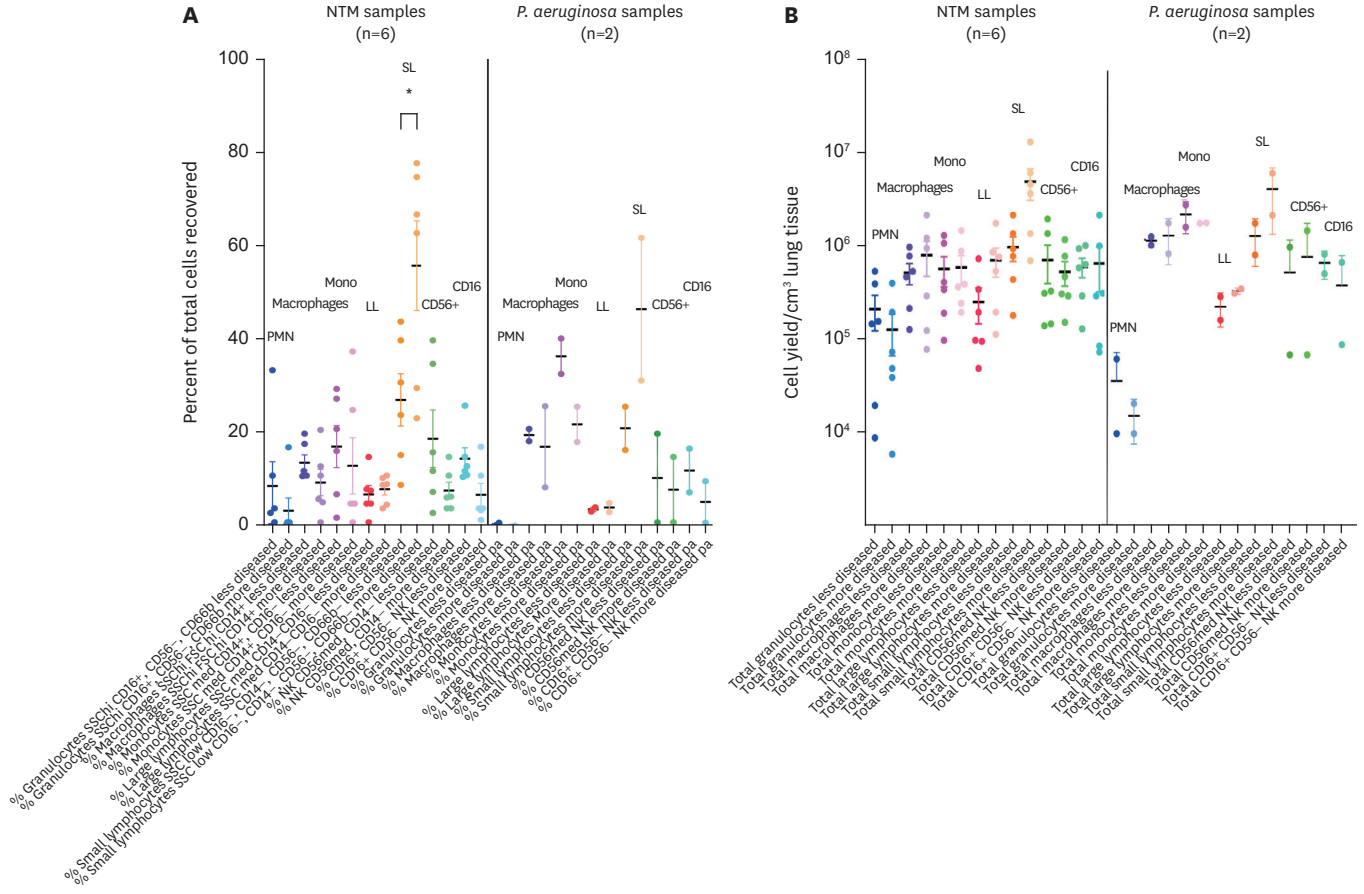

Figure 3. Flow cytometric analyses for the major leukocytes of surgical lung tissues of NTM-LD and *PsA*-LD. (A) Percentage of the indicated cell types and (B) absolute cell number per cm³ of lung tissue recovered of the major leukocytes stratified by less-diseased and more-diseased areas of the resected lung segment or lobe.
*p<0.05.

https://doi.org/10.4110/in.2022.22.e27

For the two *PsA*-LD surgical samples, neutrophils were also the least prevalent immune cells in both the less- and more-diseased samples. Indeed, neutrophils in the *PsA*-LD were not only fewer than NTM-LD, but the more-diseased areas actually had lower number of neutrophils than the less-diseased samples albeit only two *PsA*-LD samples were analyzed. We also confirmed, using CD66b, that there were very few neutrophils compared to other subsets (data not shown). There were no differences in the number of macrophages, monocytes, and large lymphocyte populations but there was greater number of small and large lymphocytes in the more-diseased tissues of the *PsA*-LD samples.

Analyzing in greater depth the lymphocyte population in the NTM-LD samples, there were no significant differences in the percentage of the T cell subtypes between the less- and more-diseased areas (**Fig. 4A**); however, generally, there were greater absolute numbers of $CD4^+$ T cells, $CD8^+$ T cells, and gamma-delta T cells in the more-diseased than the less-diseased tissues (**Fig. 4B**). $CD19^+$ B cells varied widely but there was significantly greater percentage of B lymphocytes and a clear trend toward greater absolute numbers in the more-diseased areas (**Fig. 4A and B**). Both $CD16^+$ and $CD56^+$ NK cells could be found in large numbers, but there no significant difference between the less- and more-diseased tissues. For the *PsA*-LD samples, there was relatively fewer $CD4^+$ T cells, $CD8^+$ T cells, gamma-delta T cells, and B cells (compared to the NTM-LD tissues) with no difference between the less-diseased vs. more-diseased tissues. The number of $CD16^+$ and $CD56^+$ NK cells in the *PsA*-LD tissues were similar to that for NTM-LD samples but such comparisons are preliminary given only two *PsA*-LD samples were available.

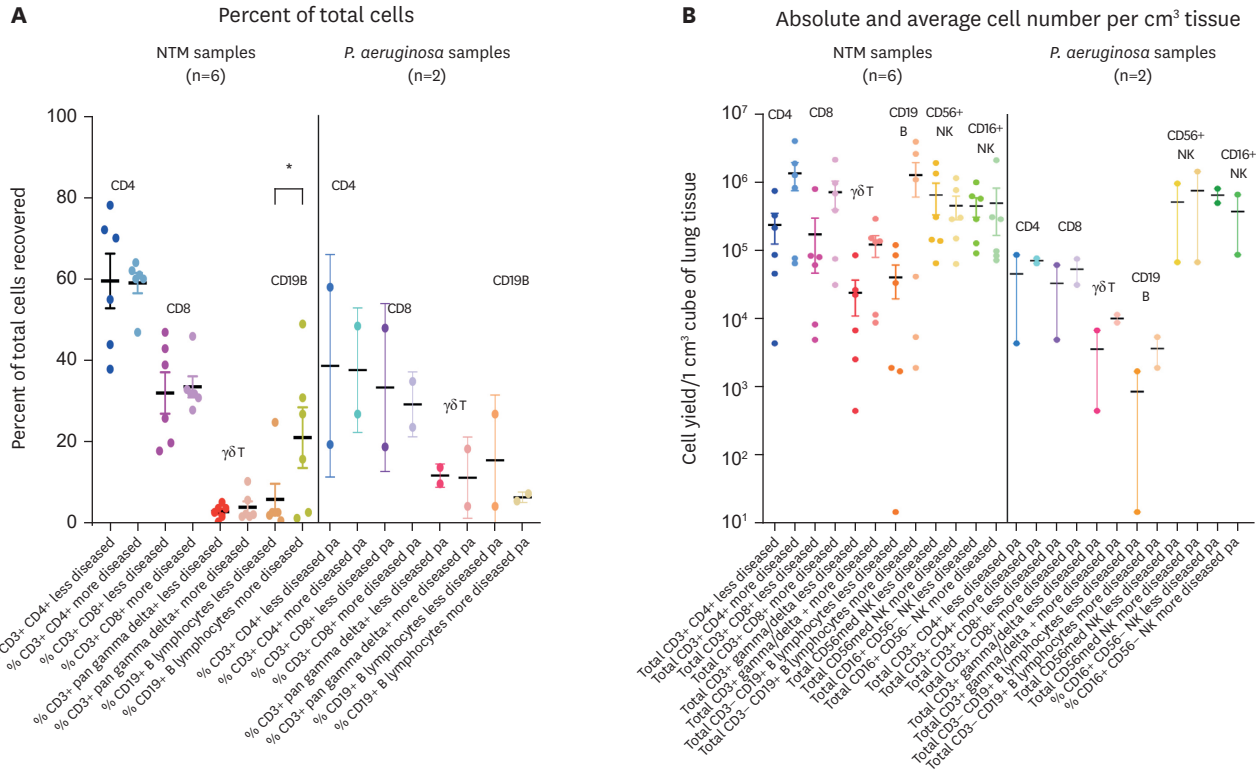

Figure 4. Flow cytometric analyses for the major lymphocyte subtypes of surgical lung tissues of NTM-LD and *PsA*-LD. (A) Percentage of the indicated cell types and (B) absolute cell number per cm^3 of lung tissue recovered of the major lymphocyte subtypes stratified by less-diseased and more-diseased areas of the resected lung segment or lobe.
*$p<0.05$.

https://doi.org/10.4110/in.2022.22.e27

Han et al. (14) determined the phenotype of blood $CD4^+$ T cells in 71 patients with NTM-LD due to MAC and 20 healthy controls following stimulation of their PBMC with heat-killed MAC. Compared to cells from control subjects, the stimulated PBMC of patients with MAC lung disease had decreased total $CD4^+$ T cells and decreased T_H17 cells but there were increased number of T_H2 cells ($CD4^+IL\text{-}4^+$), Tregs, and $CD4^+$ T cells that expressed deactivation or exhaustion markers PD-1, CTLA-4, and TIM-3. While this study of blood cells provides a systemic glimpse into the distribution of $CD4^+$ T cell phenotypes, it does not provide information on what is happening in the lung compartment. Another limitation of this study (and ours) is that because the analyses of blood (and tissues) were done in individuals with established NTM-LD, we are unable to answer whether differential infiltration of these cellular phenotypes were present before the initial infection or whether they were the result of the infection. However, an advantage of profiling blood immune cells is that it provides an opportunity to phenotype over time the immune cells during the disease course, an endeavor not feasible by repeated lung tissue biopsies.

A semi-invasive way to assess the cell types in the lungs is by BAL, providing a means to analyze the detachable cells in the medium/smaller size airways and the alveolar space. With either localized or military tuberculosis, BAL have demonstrated increased percentage of neutrophils and lymphocytes as well as relative decrease in macrophages; in contrast, the peripheral blood showed the opposite pattern of decreased number of lymphocytes and increased number of monocytes (15,16). In addition, there was found a higher percentage in the BAL of $CD4^+$ T cells and lower percentage $CD8^+$ T cells (and opposite findings in peripheral blood) of patients with higher clinical grade of pulmonary tuberculosis – defined by extent of lung involvement and presence of fever and weight loss (17). NTM-LD is typically associated with relative increased percentage of lymphocytes and neutrophils in the BAL fluid (18). With MAC-associated nodular bronchiectasis, patients who were "not deteriorating" (n=8) had increased lymphocyte and neutrophils but macrophages remained the dominant cell population; i.e., macrophages > lymphocytes > neutrophils; in contrast, of those who were "deteriorating" (n=13), the relative percentages were neutrophils ≥ macrophages > lymphocytes (12). In 37 MAC lung disease subjects, those with neutrophil-dominant BAL had more severe radiographic disease and greater clinical deterioration than those with lymphocyte-dominant BAL (19).

In our analysis of the lung tissues of those with chronic NTM-LD, we predicted the presence of abundant inflammatory cells typically associated with chronic infections such as macrophages and lymphocytes but also neutrophils given the purulent nature of expectorated sputa and associated bronchiectasis. We found a substantial infiltration of lymphocytes into heavily diseased tissue, across the whole spectrum in most cases, and fewer neutrophils. This distribution pattern is consistent with the chronic nature of NTM-LD in our patients. Furthermore, despite the severity of the localized lung disease in the patients examined, clinical control of the infection with antibiotics is a prerequisite prior to lung resection. This clinical stipulation may also account for the fewer neutrophils found; i.e., the NTM infections in our patients were under control and surgery was performed to remove the irreversibly destroyed lung tissue, a potential nidus for future infections. The presence of clusters of $CD4^+$ T cells, $CD8^+$ T cells, and NK lymphocytes, their relatively small size, and dense nuclear stain all suggest that these cells are recent immigrants and perhaps is a *de novo* lymphocytic tissue organization, possibly a pseudo-lymphoid follicle.

Future studies should examine the subtypes of macrophages and dendritic cells but also for T and B cell immunophenotypes, including aged B cells, which have been found in increased

number in the BAL of patients with sarcoidosis, beryllium disease, and hypersensitivity pneumonitis and may play a role in the pathogenesis of these granulomatous disease (20). "M1" (IFN/IL-12) skewed macrophages are considered to be host-protective through their effector functions of killing mycobacteria, participating in granuloma formation, and orchestrating other components of the immune system via presenting Ags and elaborating cytokines and chemokines that recruit and activate other cell types. The alternatively activated "M2 subtypes" are also important in a temporal fashion because they are necessary to dampen the immune response and repair the lung injury once the infection is under control. A similar paradigm may be made for the T effector cells such as the T_H1 and T_H17 cells that are necessary during the acute phase of the infection and the T_H2 and Tregs that are required to quell the inflammation once bacterial killing is achieved. The high numbers of CD8 T cells and NK cells in these tissues suggests a T_H1 response, but it's not clear why they would persist if they are indeed skewed to this phenotype. Given the large amount of tissue destruction, perhaps they are still active. There are also regions of fibrosis. There is evidence that T_H2, T_H17, and Tregs contribute to alternative activation of macrophages (21-23), perhaps contributing to the chronic inflammation and airway fibrosis that is typically seen on CT scans and lung tissues of patients with NTM-LD.

Clearly there is a role for NK cells in the immune response in the lungs (24), and by the nature of the cytotoxicity, they may be major inducers of the massive destruction seen in both chronic NTM-LD and *PsA*-LD pathology. Future studies can also examine the four phenotypes of NK cells that have been described thus far (24). It is also important to note that some $CD56^+$ and $CD16^+$ cell types are not NK cells, but other lymphocytes. Likewise, a more detailed analysis of the sub-populations and phenotypes of all lymphocytes in this response would likely yield much greater insight into the immune response and potential therapeutic targets.

While it would be informative to have analysis of earlier lesions of NTM-LD, it is uncommon to have surgical biopsies of such lesions but even if they are available, allocation of the small pieces of lung tissues for clinical pathological analysis will likely result in inadequate amount of tissues available for research use. However, correlating the cellular phenotype of blood, BAL, and surgical lung tissue will likely be informative but the BAL will have to be done at least one week prior to the surgery or immediately prior to surgery (in the operating room) as the saline instillation itself for the BAL may incite an inflammatory response. While the value of blood analysis is that it can be obtained much earlier in the course of the illness and prospectively followed, the disadvantage is that it is not the lung environment.

In summary, in stable NTM-LD patients who underwent lung resection to remove a potential nidus for future exacerbations, the lung tissues contained significantly more small lymphocytes than macrophages or monocytes, and both cell populations outnumbered the neutrophils. The lymphocyte population of $CD4^+$ T cells, $CD8^+$ T cells, gamma-delta T cells, and B cells were also more prevalent in the more-diseased tissues but there was no such differential distribution in the NK cells.

SUPPLEMENTARY MATERIALS

Supplementary Figure 1

Patient A, NTM-LD. (A) Axial, (B) coronal, and (C) sagittal CT images showing a small cavity in the posterior right upper lobe (white arrows) with adjacent linear atelectasis. The latter two images also show scattered areas of ground glass nodular opacities. Photomicrographs show (D) nodular area of fibrosis surrounding a dilated bronchiole (circled), (E) a higher power view of a dilated bronchiole (white arrow), and (F) necrotizing granuloma (white arrow) with central loss of necrotic material.

Click here to view

Supplementary Figure 2

Patient B, NTM-LD. (A) Axial, (B) coronal, and (C) sagittal CT images showing fibrocavitary disease of the left upper lobe (black arrow) with evidence of volume loss of the left lung and traction of the left hemidiaphragm. Photomicrographs show (D) a dilated bronchus (asterisk) with surrounding fibrosis and chronic inflammation, (E) necrotizing granuloma with layers of necrosis (large white arrow), epithelioid histiocytes (thin black arrows) and surrounding fibrosis and chronic inflammation, and (F) higher power view of necrotizing granuloma with central eosinophilic necrosis cuffed by epithelioid histiocytes and multinucleated giant cells. There is collagenous fibrosis surrounding the granuloma.

Click here to view

Supplementary Figure 3

Patient C, NTM-LD. (A) Axial, (B) coronal, and (C) sagittal CT images showing right lower lobe bronchiectasis with scattered areas of coalescing small to medium sized nodules (white arrow). Photomicrographs demonstrate (D) numerous coalescing, necrotizing granulomas and (E) in a higher power view, a large area of central necrosis surrounded by epithelioid histiocytes and multinucleated giant cells.

Click here to view

Supplementary Figure 4

Patient D, NTM-LD. (A) Axial CT image shows bronchiectasis and atelectasis of the left lower lobe and bronchiectasis of the right middle lobe. (B) Coronal and (C) sagittal images demonstrate the extensive left lower lobe bronchiectasis and atelectasis. Photomicrographs show (D) numerous necrotizing granulomas (asterisks) surrounded by fibrosis and chronic inflammation, (E) necrotizing granuloma surrounded by epithelioid histiocytes, multinucleated giant cells and fibrosis. Note the adjacent pulmonary artery (thin black arrow), and a (F) high power view of a granuloma demonstrating the heavily collagenized center.

Click here to view

Supplementary Figure 5

Patient E, NTM-LD. (A) Axial, (B) coronal, and (C) sagittal CT images showing severe bronchiectasis and atelectasis of the right middle lobe and lingula. Photomicrographs reveal (D) a dilated airway with chronic inflammation of the wall, including lymphoid aggregates (circle) and nonnecrotizing granulomas (inset—black arrows), and (E) dilated,

ectatic airway with inspissated mucus and inflammatory debris (inset shows high power of luminal debris).

Click here to view

Supplementary Figure 6

Patient F, NTM-LD. (A) Axial, (B) coronal, and (C) sagittal CT images showing bronchiectasis, patchy areas of ground glass opacities, and centrilobular nodules in the right middle lobe, and severe bronchiectasis of the lingula with localized central bronchiectasis. Photomicrographs demonstrate (D) peripheral area of fibrosis (note the pleural surface – thin black arrows) surrounding mildly dilated small airway with lymphoid aggregates in the walls, (E) a dilated small airway filled with inflammatory debris, and (F) a high power of inflammatory debris, which include neutrophils.

Click here to view

Supplementary Figure 7

Patient G, *PsA*-LD. (A) Axial, (B) coronal, and (C) sagittal CT images showing bronchiectasis of the right middle lobe, and bilateral central bronchiectasis. Photomicrographs reveal (D) dilated bronchiole (note the smaller accompanying pulmonary artery—thin arrow), surrounded by collagenous fibrosis, (E) higher power of the same dilated airway show chronic inflammation of the wall, and (F) an even higher power of the dilated airway wall showing intraluminal neutrophils and cellular debris.

Click here to view

Supplementary Figure 8

Patient H, *PsA*-LD. (A) Axial, (B) coronal, and (C) sagittal CT images showing diffuse bronchiectasis and patchy areas of ground glass opacities of the left lower lobe and milder central bronchiectasis of the right lower lobe. Photomicrographs reveal (D) peripheral area of dense fibrosis with a dilated small airway (white arrow), (E) higher power of the dilated lumen containing inflammatory debris, and (F) high power of the inflammatory debris with evidence of necrosis.

Click here to view

REFERENCES

1. Fujita J, Ohtsuki Y, Suemitsu I, Shigeto E, Yamadori I, Obayashi Y, Miyawaki H, Dobashi N, Matsushima T, Takahara J. Pathological and radiological changes in resected lung specimens in *Mycobacterium avium intracellulare* complex disease. *Eur Respir J* 1999;13:535-540.
PUBMED | CROSSREF
2. Kim TS, Koh WJ, Han J, Chung MJ, Lee JH, Lee KS, Kwon OJ. Hypothesis on the evolution of cavitary lesions in nontuberculous mycobacterial pulmonary infection: thin-section CT and histopathologic correlation. *AJR Am J Roentgenol* 2005;184:1247-1252.
PUBMED | CROSSREF
3. Moore EH. Atypical mycobacterial infection in the lung: CT appearance. *Radiology* 1993;187:777-782.
PUBMED | CROSSREF
4. Yu JA, Pomerantz M, Bishop A, Weyant MJ, Mitchell JD. Lady Windermere revisited: treatment with thoracoscopic lobectomy/segmentectomy for right middle lobe and lingular bronchiectasis associated

with non-tuberculous mycobacterial disease. *Eur J Cardiothorac Surg* 2011;40:671-675.
PUBMED | CROSSREF

5. Mitchell JD. Surgical treatment of pulmonary nontuberculous mycobacterial infections. *Thorac Surg Clin* 2019;29:77-83.
PUBMED | CROSSREF
6. Jarand J, Levin A, Zhang L, Huitt G, Mitchell JD, Daley CL. Clinical and microbiologic outcomes in patients receiving treatment for *Mycobacterium abscessus* pulmonary disease. *Clin Infect Dis* 2011;52:565-571.
PUBMED | CROSSREF
7. Pezzia W, Raleigh JW, Bailey MC, Toth EA, Silverblatt J. Treatment of pulmonary disease due to *Mycobacterium kansasii*: recent experience with rifampin. *Rev Infect Dis* 1981;3:1035-1039.
PUBMED | CROSSREF
8. Jeon K, Kwon OJ, Lee NY, Kim BJ, Kook YH, Lee SH, Park YK, Kim CK, Koh WJ. Antibiotic treatment of *Mycobacterium abscessus* lung disease: a retrospective analysis of 65 patients. *Am J Respir Crit Care Med* 2009;180:896-902.
PUBMED | CROSSREF
9. Daley CL, Iaccarino JM, Lange C, Cambau E, Wallace RJ Jr, Andrejak C, Böttger EC, Brozek J, Griffith DE, Guglielmetti L, et al. Treatment of nontuberculous mycobacterial pulmonary disease: an official ATS/ERS/ESCMID/IDSA clinical practice guideline. *Clin Infect Dis* 2020;71:905-913.
PUBMED | CROSSREF
10. Fox GJ, Mitnick CD, Benedetti A, Chan ED, Becerra M, Chiang CY, Keshavjee S, Koh WJ, Shiraishi Y, Viiklepp P, et al. Collaborative group for meta-analysis of individual patient data in MDR-TB. Surgery as an adjunctive treatment for multi-drug resistant tuberculosis: an individual patient data meta-analysis. *Clin Infect Dis* 2016;62:887-895.
PUBMED | CROSSREF
11. Chan ED, Laurel V, Strand MJ, Chan JF, Huynh ML, Goble M, Iseman MD. Treatment and outcome analysis of 205 patients with multidrug-resistant tuberculosis. *Am J Respir Crit Care Med* 2004;169:1103-1109.
PUBMED | CROSSREF
12. Yamazaki Y, Kubo K, Takamizawa A, Yamamoto H, Honda T, Sone S. Markers indicating deterioration of pulmonary *Mycobacterium avium-intracellulare* infection. *Am J Respir Crit Care Med* 1999;160:1851-1855.
PUBMED | CROSSREF
13. Tighe RM, Redente EF, Yu YR, Herold S, Sperling AI, Curtis JL, Duggan R, Swaminathan S, Nakano H, Zacharias WJ, et al. Improving the quality and reproducibility of flow cytometry in the lung. An Official American Thoracic Society Workshop Report. *Am J Respir Cell Mol Biol* 2019;61:150-161.
PUBMED | CROSSREF
14. Han SA, Ko Y, Shin SJ, Jhun BW. Characteristics of circulating $CD4^+$ T cell subsets in patients with *Mycobacterium avium* complex pulmonary disease. *J Clin Med* 2020;9:E1331.
PUBMED | CROSSREF
15. Ozaki T, Nakahira S, Tani K, Ogushi F, Yasuoka S, Ogura T. Differential cell analysis in bronchoalveolar lavage fluid from pulmonary lesions of patients with tuberculosis. *Chest* 1992;102:54-59.
PUBMED | CROSSREF
16. Sharma SK, Pande JN, Verma K. Bronchoalveolar lavage (BAL) in miliary tuberculosis. *Tubercle* 1988;69:175-178.
PUBMED | CROSSREF
17. Tsao TC, Chen CH, Hong JH, Hsieh MJ, Tsao KC, Lee CH. Shifts of T4/T8 T lymphocytes from BAL fluid and peripheral blood by clinical grade in patients with pulmonary tuberculosis. *Chest* 2002;122:1285-1291.
PUBMED | CROSSREF
18. Yamazaki Y, Kubo K, Sekiguchi M, Honda T. Analysis of BAL fluid in *M. avium-intracellulare* infection in individuals without predisposing lung disease. *Eur Respir J* 1998;11:1227-1231.
PUBMED | CROSSREF
19. Inomata T, Konno S, Nagai K, Suzuki M, Nishimura M. Neutrophil predominance in bronchoalveolar lavage fluid is associated with disease severity and progression of HRCT findings in pulmonary *Mycobacterium avium* infection. *PLoS One* 2018;13:e0190189.
PUBMED | CROSSREF
20. Phalke S, Aviszus K, Rubtsova K, Rubtsov A, Barkes B, Powers L, Warner B, Crooks JL, Kappler JW, Fernández-Pérez ER, et al. Age-associated B cells appear in patients with granulomatous lung diseases. *Am J Respir Crit Care Med* 2020;202:1013-1023.
PUBMED | CROSSREF
21. Gieseck RL 3rd, Wilson MS, Wynn TA. Type 2 immunity in tissue repair and fibrosis. *Nat Rev Immunol* 2018;18:62-76.
PUBMED | CROSSREF

22. Paun A, Bergeron ME, Haston CK. The Th1/Th17 balance dictates the fibrosis response in murine radiation-induced lung disease. *Sci Rep* 2017;7:11586.
PUBMED | CROSSREF

23. Chakraborty K, Chatterjee S, Bhattacharyya A. Impact of Treg on other T cell subsets in progression of fibrosis in experimental lung fibrosis. *Tissue Cell* 2018;53:87-92.
PUBMED | CROSSREF

24. Theresine M, Patil ND, Zimmer J. Airway natural killer cells and bacteria in health and disease. *Front Immunol* 2020;11:585048.
PUBMED | CROSSREF